J. Fluid Mech. (1985), *vol.* 158, *pp.* 219–244
Printed in Great Britain

Creeping motion of a sphere through a Bingham plastic

By A. N. BERIS, J. A. TSAMOPOULOS, R. C. ARMSTRONG AND R. A. BROWN

Department of Chemical Engineering, Massachusetts Institute of Technology, Cambridge, MA 02139

(Received 28 November 1984 and in revised form 8 March 1985)

A solid sphere falling through a Bingham plastic moves in a small envelope of fluid with shape that depends on the yield stress. A finite-element/Newton method is presented for solving the free-boundary problem composed of the velocity and pressure fields and the yield surfaces for creeping flow. Besides the outer surface, solid occurs as caps at the front and back of the sphere because of the stagnation points in the flow. The accuracy of solutions is ascertained by mesh refinement and by calculation of the integrals corresponding to the maximum and minimum variational principles for the problem. Large differences from the Newtonian values in the flow pattern around the sphere and in the drag coefficient are predicted, depending on the dimensionless value of the critical yield stress Y_g below which the material acts as a solid. The computed flow fields differ appreciably from Stokes' solution. The sphere will fall only when Y_g is below 0.143. For yield stresses near this value, a plastic boundary layer forms next to the sphere. Boundary-layer scalings give the correct forms of the dependence of the drag coefficient and mass-transfer coefficient on yield stress for values near the critical one. The Stokes limit of zero yield stress is singular in the sense that for any small value of Y_g there is a region of the flow away from the sphere where the plastic portion of the viscosity is at least as important as the Newtonian part. Calculations for the approach of the flow field to the Stokes result are in good agreement with the scalings derived from the matched asymptotic expansion valid in this limit.

1. Introduction

Viscoplastic fluids combine the behaviour of rigid solids and non-Newtonian viscous liquids by differentiating between physical regions where these descriptions hold according to criteria based on the level of stress in the material. For low stress values the material will not deform, but beyond some critical value it flows as an inelastic non-Newtonian fluid. The fluid mechanics, as well as mass and heat transport, of viscoplastic materials is becoming increasingly important, especially with the discovery that many multicomponent fluids, such as foams, slurries, suspensions, emulsions and fermentation broths, are viscoplastic.

The Bingham-plastic constitutive equation (Bingham 1922; Oldroyd 1947*a*) is the most often used model for a viscoplastic material. Here regions of rigid-solid and inelastic-fluid behaviour are separated in terms of von Mises' yield condition. The

constitutive equation relating the deviatoric stress $\boldsymbol{\tau}^*$ and rate-of-strain $\dot{\boldsymbol{\gamma}}^*$ tensors is given as (Oldroyd 1947*a*; Bird, Armstrong & Hassager 1977)

$$\boldsymbol{\tau}^* = \left(\eta_0 + \frac{\tau_y}{\dot{\gamma}^*}\right)\dot{\boldsymbol{\gamma}}^* \quad (\tau^* > \tau_y), \tag{1.1a}$$

$$\dot{\boldsymbol{\gamma}}^* = \mathbf{0} \quad (\tau^* \leqslant \tau_y), \tag{1.1b}$$

where τ^* and $\dot{\gamma}^*$ are the second invariants of the tensors, defined as

$$\tau^* \equiv [\tfrac{1}{2}\boldsymbol{\tau}^* : \boldsymbol{\tau}^*]^{\frac{1}{2}}, \quad \dot{\gamma}^* \equiv [\tfrac{1}{2}\dot{\boldsymbol{\gamma}}^* : \dot{\boldsymbol{\gamma}}^*]^{\frac{1}{2}}, \tag{1.2}$$

and η_0 and τ_y are called the plastic viscosity and the yield stress respectively. Equations (1.1*a*, *b*) define two distinct regions of flow. In the first the invariant τ^* exceeds the yield stress and the material flows with a non-Newtonian viscosity function defined as $\eta(\dot{\gamma}^*) \equiv \eta_0 + \tau_y/\dot{\gamma}^*$. In the second the stress is less than the yield value and the material behaves as a rigid solid. The fluid and solid regions are separated by a distinct yield surface.

The composite form of the viscosity points to an important characteristic of viscoplastic flows. When the shear rates are large so that $\dot{\gamma}^* \gg \tau_y/\eta_0$ the fluid behaves as a Newtonian liquid; however, as $\dot{\gamma}^*$ becomes small the plastic contribution $\tau_y/\dot{\gamma}^*$ will become important, irrespective of the magnitude of the yield stress. This idea is crucial to understanding the asymptotic behaviour of complex flows as the yield stress tends either to very small values or to the critical value for a rigid plastic material. Although substantial research has been directed at deriving closed-form solutions for Bingham fluids in rectilinear and lubrication flows (see Bird, Dai & Yarusso 1983), few solutions have been presented for complex flows with streamlines that are not rectilinear. The most notable omission is the calculation of the creeping flow about a sphere in a large sea of fluid, where the formation of a rigid plastic region around the sphere has very pronounced effects on the flow field. Our aim is to present a rigorous numerical solution for this problem, and in doing so to supply an algorithm for the calculation of other viscoplastic flows. Besides being of practical importance in understanding the fluid mechanics and species transport in this abundant class of materials, these calculations may form a basis for a new method of measuring the material properties η_0 and τ_y used in the Bingham constitutive model.

Volarovich (1953) was the first to realize that a sphere falling in a Bingham plastic must do so in a small envelope of fluid separating the body from rigid solid in which the stress does not exceed the yield criterion. Valentic & Whitmore (1965) put forth a crude approximation for the fall velocity of a sphere by using the idea of Andres (1960) that the solid is surrounded by a liquid 'sphere of influence' over which only viscous forces cause drag. Other regions of solid can exist for an object falling in a Bingham plastic. For example, the stagnation points that must exist in the flow at the front and back of the sphere guarantee that solid must form in these regions for any finite value of the yield stress, as recognized by Yoshioka, Adachi & Ishimura (1971).

The fluidity of the material adjacent to the sphere is a result of the stress created by the sphere's weight. No motion is expected for nearly neutrally buoyant particles. The state of incipient motion defines a critical yield stress that can be estimated by calculations for an ideal rigid plastic with a yield criterion (see Hill 1950). Then the onset of fluid motion corresponds to the development of a slip surface in the plastic material. Axisymmetric problems in ideal plasticity, like the one needed to consider

a suspended sphere, are governed by elliptic-equation sets (Symonds 1949) and have not been solved previously. In planar geometries, the analogous equations are hyperbolic, and slip lines develop along the characteristic direction in which the material undergoes purely shear deformation, with the magnitude of the stress equal to the yield value. The motion of the sphere appears as a discontinuity in the velocity along this slip surface. Symmetry conditions can force slip lines to intersect planes where the motion must be pure compression or extension, as is the case along the axis of motion of a sphere. Slater (1977) has shown that the yield surface in a planar geometry must meet the symmetry plane at an angle of $\frac{1}{4}\pi$. No extension of this result to an axisymmetric problem is available.

Oldroyd (1947*b*) developed a plastic boundary-layer theory to splice together the discontinuity in velocity predicted for an ideal rigid plastic material and the concept of fluidity in a Bingham viscoplastic model. He envisioned the fluid region to be divided into two parts: a thin layer adjacent to the solid in which both viscous and yield stresses were important, and a region next to the rigid plastic in which the yield-stress term in the viscosity was dominant. He termed the first region adjacent to the solid a plastic boundary layer and scaled the field equations and boundary conditions accordingly. We extend this analysis to the axisymmetric flow around a sphere to determine the proper scalings near the critical yield-stress value.

Several experimental investigations have been reported for the flow around a sphere falling in viscoplastic fluids (dy Plessis & Ansley 1967; Ansley & Smith 1967; Ito & Kajiachi 1969). These concentrated on measuring the drag coefficient for the sphere as a function of τ_y and η_0 for the fluid, and produced relationships between the drag coefficient and the effective Reynolds number. To do this, the ratio of viscous to yield forces acting on the sphere had to be established to correlate the results with Reynolds number. The ratio either was taken to be dependent on the value of the yield stress and was fitted experimentally (Ito & Kajiachi 1969), or was assumed to be constant and determined by analysis (Ansley & Smith 1967). To do this, Ansley & Smith borrowed ideas from the theory of two-dimensional slip lines in a rigid plastic and approximated the yield surface for a viscoplastic material as a toroid centred at the equator of the sphere with radius $R_0\sqrt{2}$, where R_0 is the radius of the sphere. The accuracy of this approximation is discussed later along with a comparison to the data for drag coefficient.

A number of authors (Prager 1954; Yoshioka & Adachi 1971; Yoshioka *et al.* 1974; Duvault & Lions 1976) have developed variational principles which hold for the inertialess flow of a Bingham fluid. Yoshioka *et al.* (1974) used them to compute upper and lower bounds on the drag coefficient. The accuracy of these computations was poor – the bounds differed by 50% – because of the crude forms used for the approximations to the velocity and stress fields and the shapes of the yield surfaces. Glowinski, Lions & Tremoliers (1981) were the first to use variational methods systematically to compute viscoplastic flows accurately by combining variational inequalities with either finite-element or finite-difference numerical approximations and effective minimization techniques. The application of these methods has been limited to the calculation of the rectilinear flows in circular and rectangular ducts and two-dimensional confined flows. Bercovier & Engelman (1980) developed a finite-element/penalty-function method for computing the flow of an inelastic fluid with a viscosity chosen to model the behaviour of a Bingham plastic by replacing rigid plastic regions with an extremely viscous fluid past a transition in the shear rate. Although this approach eliminated the need for the calculation of the exact location of the yield surfaces, it introduced the complication that fine finite-element

discretizations were needed in the *a priori* unknown regions where the artificial viscosity function increased drastically.

Approximating a Bingham plastic by an inelastic non-Newtonian fluid with a smoothly varying viscosity, as suggested by the numerical method of Bercovier & Engelman (1980) and by the analysis of lubrication flows by Lipscomb & Denn (1984), leads to the conclusion that the behaviour in flow around a sphere for a Bingham plastic with very small yield stress can be well approximated by Stokes flow. Bhavaraju, Mashelkar & Blanch (1978) formulated a regular perturbation analysis about zero yield stress and neglected the presence of yield surfaces to calculate the drag and mass transfer from a sphere in a fluid with low yield stress. Although Stokes flow certainly is a solution when the yield stress is identically zero, it is not clear that the behaviour of the solution is regular as τ_y approaches zero and that the perturbation series of Bhavaraju *et al.* is appropriate. The variational formulations have been used by Duvaut & Lions (1976) to prove that a unique solution exists for the creeping flow ($Re = 0$) of Bingham plastics in both interior and exterior domains. These authors have also proved that the solution of the Bingham-plastic problem approaches the Newtonian result as the yield stress approaches zero. However, their argument presupposes that the Newtonian result is square-integrable. This is not the case for a sphere in an unbounded fluid, and the variational result suggests that the solution for a Bingham fluid with vanishingly small yield stress should differ from the Newtonian result, at least at large distances from the sphere.

We solve for the velocity and pressure fields in the fluid portion of the Bingham material and for the shape of the yield surfaces for the creeping flow around a sphere in an unbounded Bingham plastic material. The calculations are based on a Galerkin finite-element algorithm developed for the solution of elliptic free-boundary problems (Ettouney & Brown 1983). In our formulation the field equations and boundary conditions are first transformed to a fixed domain by a mapping involving the unknown shape functions describing the locations of the yield surfaces. The new equation set for the coupled field and surface equations is reduced to a nonlinear algebraic equation set by a Galerkin/penalty finite-element formulation. This algebraic set is solved by Newton's method, which iterates simultaneously for all unknowns.

The formulation of the free-boundary problem for flow around a sphere is presented in §2 along with the variational integrals which will be used in our assessment of numerical accuracy. The finite-element analysis is described in §3. Our results for the velocity field, shapes of the yield surfaces, the drag coefficient, and a mass-transfer coefficient in the limit of high Péclet number are given in §4. The finite-element results are compared in §5 with the scalings predicted by the plastic boundary-layer theory valid for large yield stress and with a matched asymptotic analysis for small values of this parameter.

2. Formulation

We consider the creeping flow of a solid sphere of radius R_0 falling in an infinite medium that behaves rheologically as a Bingham plastic. The flow is assumed to be axisymmetric, with the sphere moving along the z-axis parallel to the direction of gravity. The flow field and shapes of the yield surfaces are represented in a spherical coordinate system (r^*, θ, ϕ) with its ori ı at the centre of the sphere. We limit our calculations to the creeping-flow limit (l = 0) so that the velocity and pressure fields have symmetry about the equatorial plane $\theta = \frac{1}{2}\pi$ and the two polar caps of solid

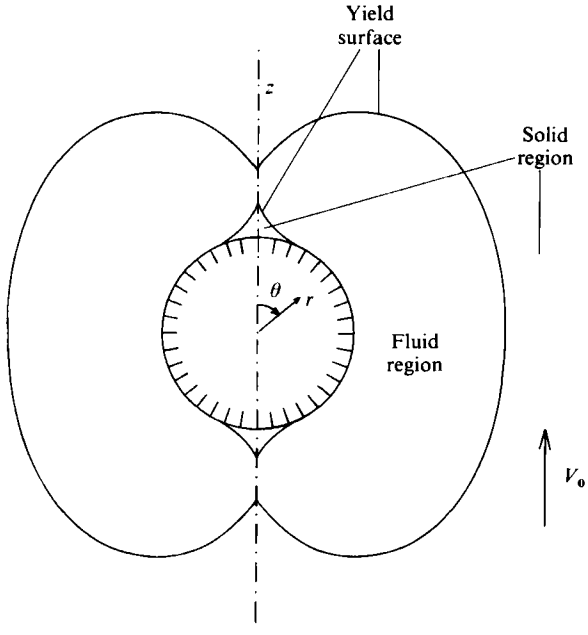

FIGURE 1. Plastic and solid regions for the flow surrounding a solid sphere falling in a Bingham plastic material.

on the sphere have identical shape. The calculations are performed in the upper-right quadrant $0 \leqslant \theta \leqslant \frac{1}{2}\pi$. The different portions of the flow domain and the yield surfaces attached to the sphere and surrounding the fluid are shown in figure 1.

Dimensionless equations are formed by scaling velocities with the fall velocity V_0 of the sphere, distances with the radius R_0 of the sphere, and pressure with the viscous stress $\eta_0 V_0/R_0$. The field equations governing the motion of the sphere are then

$$\boldsymbol{\nabla}\cdot\boldsymbol{\tau}-\boldsymbol{\nabla}P=\mathbf{0}, \tag{2.1}$$

$$\boldsymbol{\nabla}\cdot\boldsymbol{v}=0, \tag{2.2}$$

$$\boldsymbol{\tau}=\left(1+\frac{N_{\mathrm{B}}}{2\dot{\gamma}}\right)\dot{\boldsymbol{\gamma}} \quad (\tau > \tfrac{1}{2}N_{\mathrm{B}}), \tag{2.3}$$

$$\dot{\boldsymbol{\gamma}}=\mathbf{0} \quad (\tau \leqslant \tfrac{1}{2}N_{\mathrm{B}}), \tag{2.4}$$

$$C_{\mathrm{s}}=\frac{1}{3}\int_S \boldsymbol{\delta}_z\cdot(\boldsymbol{\tau}-P\boldsymbol{\delta})\cdot\boldsymbol{n}\,\mathrm{d}s, \tag{2.5}$$

where $\boldsymbol{n}$ is the unit vector normal to the surface and S is the portion of the surface of sphere exposed to the fluid and the surface of the solid caps attached at the poles, $S=\partial\hat{D}_{1,c}\cap\partial\hat{D}_{1,b}$ in figure 2. The dimensionless pressure has been modified to include the gravitational potential $\rho g z$, where ρ is the density of the fluid and g is the acceleration due to gravity. The two dimensionless numbers appearing in these equations are the Bingham number N_{B}, which measures the ratio of the strength of the yield stress to the viscous stress, and the Stokes drag coefficient C_{s}; these groups are defined as

$$N_{\mathrm{B}}\equiv\frac{2\tau_y R_0}{\eta_0 V_0}, \quad C_{\mathrm{s}}\equiv\frac{F}{6\pi\eta_0 V_0 R_0}, \tag{2.6}$$

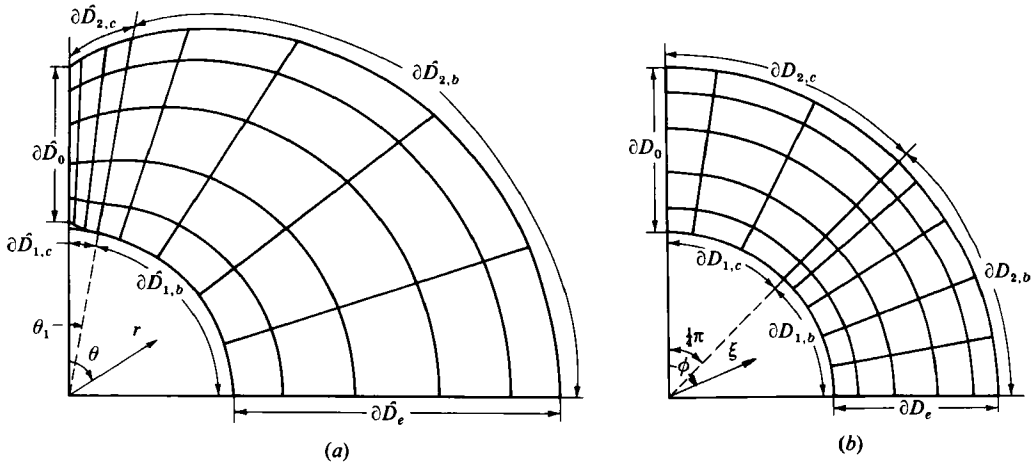

FIGURE 2. Sample finite-element mesh and notation for boundaries represented in (*a*) the original and (*b*) the transformed coordinate systems.

where F is the external force acting on the sphere. For a sphere in free fall

$$F = \tfrac{4}{3}\pi(\rho_s - \rho) R_0^2 g, \tag{2.7}$$

where ρ_s is the density of the sphere.

A third dimensionless group can be formed from the ratio of the yield stress to the externally applied force, and is called the yield-stress parameter Y_g:

$$Y_g = 2\tau_y \pi R_0^2 / F, \tag{2.8}$$

which is related to N_B and C_s by

$$N_B \equiv 6 C_s Y_g. \tag{2.9}$$

The shape of the outer yield surface surrounding the sphere and fluid is represented by the radial shape function $r = f_2(\theta)$, $0 \leqslant \theta \leqslant \frac{1}{2}\pi$, and the shape of the solid cap at the top pole of the sphere is given as $r = f_1(\theta)$, $0 \leqslant \theta \leqslant \theta_1$. The boundary conditions on the surface of the sphere and on any solid material attached to it are

$$\boldsymbol{v} = \boldsymbol{0} \quad (r = 1,\ \theta_1 \leqslant \theta \leqslant \tfrac{1}{2}\pi) \quad (r = f_1(\theta),\ 0 \leqslant \theta \leqslant \theta_1). \tag{2.10}$$

The solid material at the outer yield surface $r = f_2(\theta)$ and beyond moves rigidly according to

$$\boldsymbol{v} = -\boldsymbol{\delta}_z \quad (r = f_2(\theta),\ 0 \leqslant \theta \leqslant \tfrac{1}{2}\pi). \tag{2.11}$$

The symmetry boundary conditions on the equatorial plane are

$$\frac{\partial v_\theta}{\partial \theta} = 0, \quad v_r = 0 \quad (1 \leqslant r \leqslant f_2(\tfrac{1}{2}\pi),\ \theta = \tfrac{1}{2}\pi). \tag{2.12}$$

Equations (2.1)–(2.12) define the free-boundary problem, which is solved here in terms of the velocity and pressure fields in the fluid region and the shapes of the yield surfaces $f_1(\theta)$ and $f_2(\theta)$.

The occurrence of $\dot{\gamma}$ in the denominator of the apparent-viscosity function in (2.3) causes numerical difficulties as a yield surface is approached, since $\dot{\gamma}$ approaches zero there. To mitigate this difficulty, several authors (Bercovier & Engelman 1980;

Glowinski *et al.* 1981) have suggested introducing a 'regularization parameter' P_R into the constitutive equation as

$$\tau = \left[1 + \frac{N_B}{2(\dot{\gamma} + P_R)}\right] \dot{\gamma} \quad (\tau \geqslant \tfrac{1}{2} N_B). \tag{2.13}$$

The definition (2.4) of the boundary between the solid and fluid regions must be modified to

$$\dot{\gamma} = F(P_R, N_B) = \tfrac{1}{2}(-P_R + (P_R^2 + 2N_B P_R)^{\frac{1}{2}}) \quad (\tau = \tfrac{1}{2} N_B). \tag{2.14}$$

Glowinski *et al.* (1981) have shown that the solution of (2.1)–(2.3) with (2.13) and (2.14) converges to the solution for a Bingham plastic as $P_R \to 0$. The convergence of numerical calculations in this limit is considered in §4.

Two different formulations exist for the solution of (2.1)–(2.14) depending on the choice of independent parameters. In the first the velocity of the sphere is set by specifying N_B, and the calculation of the drag coefficient is decoupled from the other equations. In the second formulation Y_g is taken as the independent parameter, and the values of N_B and C_s are computed by solving (2.9) simultaneously with the field and constitutive equations, boundary conditions and the expression for the drag coefficient. This is the approach used in our numerical calculations.

The first formulation mentioned above is the basis for minimum and maximum principles that describe the creeping flow of a Bingham plastic (Prager 1954; Yoshioka & Adachi 1971). These two variational principles are stated as follows for a flow in a fluid volume V bordered by a surface S_V with normal $\boldsymbol{n}$ on which the velocity field is set:

Minimum principle

Among all velocity fields with piecewise-continuous first derivatives which satisfy the equation of continuity and the boundary conditions on S_V, the solution to the Bingham-flow equation minimizes the dimensional expression

$$H^* = \int_V (\eta_0 \dot{\gamma}^{*2} + 2\tau_y \dot{\gamma}^*) \, \mathrm{d}V. \tag{2.15}$$

Maximum principle

Among all stress fields with piecewise-continuous first derivatives that satisfy the equations of motion, the actual stress field $\boldsymbol{\tau}^*$ maximizes the expression

$$K^* = -\frac{1}{4} \int_V [\,|\tau^* - \tau_y| + \tau^* - \tau_y]^2 \, \mathrm{d}V + 2 \int_{SV} \boldsymbol{n} \cdot [\boldsymbol{\tau}^* \cdot \boldsymbol{v}^*] \, \mathrm{d}S. \tag{2.16}$$

Both expressions (2.15) and (2.16) take the same limiting value when evaluated with the velocity and stress fields that satisfy the Bingham-plastic constitutive equation. We use the calculation of H^* and K^* as a test of accuracy for our numerical algorithm.

3. Finite-element analysis

The free-boundary problem defined by (2.1)–(2.14), written in the spherical coordinate system (r, θ, ϕ), is transformed to a fixed domain in the non-orthogonal coordinate system (ξ, χ, ψ) shown in figure 2 by mappings involving the shape functions $f_1(\theta)$ and $f_2(\theta)$ for the two yield surfaces. The solid cap attached to the pole of the sphere is transformed to the upper fourth of a unit sphere ($\xi = 1$,

Mesh	Element distribution: azimuthal direction	Element distribution: radial direction	Number of degrees of freedom
B1	16	14	2217
B2	19	18	3320
B3	21	25	5016

TABLE 1. Finite-element meshes

$0 \leqslant \chi \leqslant \frac{1}{4}\pi$), and the outer yield surface is mapped to a spherical surface at $\xi = 2$ ($0 \leqslant \chi \leqslant \frac{1}{2}\pi$). The mappings between the original and transformed coordinates are, for $0 \leqslant \theta \leqslant \theta_1$,

$$\xi \equiv 1+\frac{r-f_1(\theta)}{f_2(\theta)-f_1(\theta)}, \quad \chi \equiv \frac{\theta\pi}{4\theta_1}, \quad \psi \equiv \phi, \tag{3.1}$$

and, for $\theta_1 \leqslant \theta \leqslant \frac{1}{2}\pi$,

$$\xi \equiv 1+\frac{r-1}{f_2(\theta)-1}, \quad \chi \equiv \frac{\pi}{4}+\frac{\pi(\theta-\theta_1)}{4(\frac{1}{2}\pi-\theta_1)}, \quad \psi \equiv \phi. \tag{3.2}$$

The equations defining the free-boundary problem can be explicitly written in the non-orthogonal coordinate system defined by (3.1)–(3.2) by constructing the base vectors, reciprocal base vectors and the gradient operator in this new system, as done by Ettouney & Brown (1983). We avoid developing these much more complicated differential equations by formulating the Galerkin weighted residual integrals for the numerical approximation using the original coordinate system (r, θ, ϕ) and then making a change of variables to (ξ, χ, ψ). The change of variables involves application of the chain rule to the derivatives arising in the original differential equations and the use of the Jacobian determinant of the transformation for the change of integration variables in the residual integrals. This scheme has the advantage that the components of velocity in the original coordinate system v_r and v_θ are kept as the dependent variables.

The transformed domain is discretized into quadrilateral elements, as shown in figure 2(*b*). The three meshes used in this analysis are listed in table 1. The intermediate mesh B2 is shown in figure 3 for the yield surfaces calculated for $Y_g = 0.1$. The components of velocity and the pressure field in the fluid region are interpolated using the biquadratic/penalty-function method developed by Bercovier & Fortin (1979) and first applied in viscoplastic calculations by Bercovier & Engelman (1980). In this approach the velocities are approximated by expansions of Lagrangian biquadratic polynomials $\{\Phi^i(\xi,\chi)\}$ as

$$\begin{bmatrix} v_r(\xi,\chi) \\ v_z(\xi,\chi) \end{bmatrix} = \sum_{i=1}^{N} \begin{bmatrix} u_i \\ v_i \end{bmatrix} \Phi^i(\xi,\chi), \tag{3.3}$$

where N is the total number of biquadratic functions, and the coefficients $\{u_i, v_i\}$ are to be determined. The pressure field in the penalty-function formulation is approximated as $P = -\lambda \nabla \cdot \boldsymbol{v}$, where λ is the penalty parameter, and is substituted into the momentum equations to eliminate P as a variable. The Galerkin weighted residual equations for the momentum equations are

$$\int_V \left[\left[1+\frac{N_B}{2(\dot{\gamma}+P_R)}\right]\dot{\boldsymbol{\gamma}}+\lambda(\nabla\cdot\boldsymbol{v})\,\boldsymbol{\delta}\right]:\nabla(\boldsymbol{\delta}_k\Phi^i)\,\mathrm{d}V = 0, \tag{3.4}$$

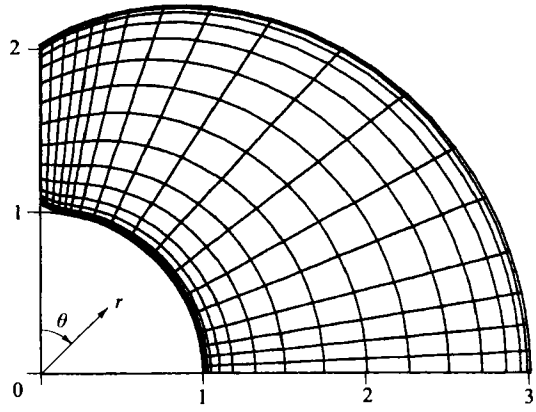

FIGURE 3. The finite-element mesh B2 in the original coordinate system for the calculation with $Y_B = 0.1$.

where $k = r$ and θ, for the two components of the momentum equation, and $\boldsymbol{\delta}$ is the unit tensor. All integrals in (3.4) are evaluated using 16-point Gaussian quadrature in each element, except the term involving λ, where 4-point quadrature is used, as suggested by Bercovier & Engelman (1979). When this reduced numerical integration is applied to the resulting term in the Galerkin equations, these authors show that the penalty formulation converges to the weak solution of the creeping-flow equations as λ^{-1} approaches zero. Bercovier & Engelman (1979) also suggest taking $\lambda^{-1} = 0.01h^2$, where h is a characteristic length for the element spacing. We found that using $\lambda^{-1} = 1 \times 10^{-5}$ for the coarse mesh B1 and 1×10^{-6} for finer meshes B2 and B3 reproduced the exact solution for Stokes flow around a sphere within a relative error of less than 0.1 %.

The shapes of the yield surfaces are approximated by expansions of one-dimensional Lagrangian quadratic functions $\{X^i(\chi)\}$ as

$$f_1(\theta) = \sum_{i=1}^{M_1} f_{1i} X^i(\chi), \quad f_2(\theta) = \sum_{i=1}^{M_2} f_{2i} X^i(\chi), \tag{3.5}$$

where M_1 and M_2 are the numbers of quadratic functions defined along each yield surface. The unknown coefficients $\{f_{1i}, f_{2i}\}$ in the expansions (3.5) are found by forcing the residual equations formed from the yield criterion (2.14) to zero on each surface:

$$\int_{S_y} (\dot{\gamma} - F(P_R, N_B))\, X^i \, dS = 0, \tag{3.6}$$

where $F(P_R, N_B)$ is defined in (2.14) and S_y is either the cap $(\partial \hat{D}_{c,1})$ or the outer $(\partial \hat{D}_{c,2} \cap \partial \hat{D}_{b,2})$ yield surface. The contributions to these integrals from each element along the boundary are evaluated using four-point Gaussian quadrature.

Introducing the regularization parameter into the constitutive equation prevents the velocity field from strictly satisfying the condition that $\dot{\gamma} = 0$ on either yield surface at $\theta = 0$. We account for this by placing a ray of small ($0 \leqslant \chi \leqslant 0.01$) elements next to the axis of symmetry and specifying the slopes $df_1/d\chi$ and $df_2/d\chi$ of the yield surfaces to be zero in these elements, instead of using (3.6). A reduction in the angular size of these elements by a factor of two ($0 \leqslant \chi \leqslant 0.005$) had no perceptible effect on the finite-element results. The angle of attachment θ_1 of the solid cap to the sphere is determined by applying the yield criterion (2.14) exactly at $\theta = \theta_1$ on the sphere.

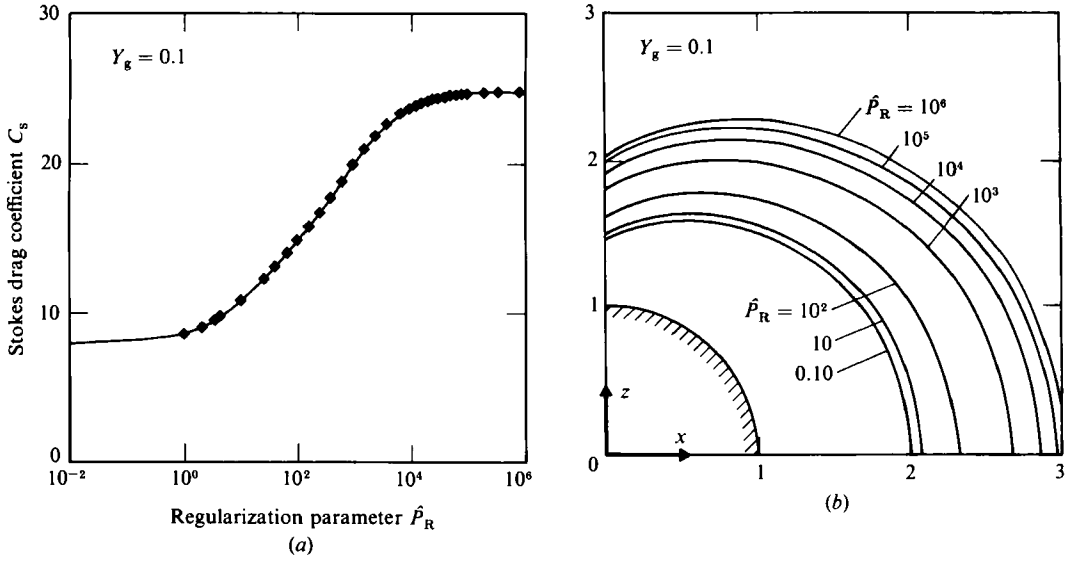

FIGURE 4. Dependence of (*a*) drag coefficient C_s and (*b*) shape of the outer yield surface $f_2(\theta)$ on the value of the regularization parameter $\hat{P}_R$.

The value of the drag coefficient C_s was determined from the integral (2.5) using the pressure field determined from the finite-element velocity field by the smoothing procedure suggested by Hughes, Liu & Brooks (1979). This method consists of forcing to zero the modified weighted residual equations formed as

$$\int_V (P + \lambda \nabla \cdot \boldsymbol{v}) \psi^i \, dV = 0, \tag{3.7}$$

where $\psi^i(\xi, \chi)$ is a bilinear Lagrangian basis function, and the pressure field $P(\xi, \chi)$ is interpolated in the finite-element form

$$P(\xi, \chi) = \sum_{i=1}^{L} P_i \psi^i(\xi, \chi). \tag{3.8}$$

This procedure gave estimates for the pressure field in Stokes flow accurate to within one percent relative error.

The entire set of nonlinear algebraic equations formed from the residual equations (3.4), (3.6) and (3.7) along with the boundary conditions on velocity determine the coefficients $\{u_i, v_i, P_i, f_{1i}, f_{2i}, C_s, \theta_1\}$ for given values of Y_g and P_R. This $(2(N+1)+M_1+M_2+L)$-dimensional equation set is represented here as

$$\mathrm{R}(\boldsymbol{u}, \boldsymbol{v}, \boldsymbol{P}, \boldsymbol{f}_1, \boldsymbol{f}_2, C_s, \theta_1; Y_g, P_R) = \boldsymbol{0}, \tag{3.9}$$

and is solved by Newton's method with the partial derivatives in the Jacobian matrix computed by analytical differentiation of the residual equations, as described by Ettouney & Brown (1983). The linear equation set at each Newton iteration was solved by Gaussian elimination using a version of Hood's (1976) frontal storage technique modified specifically for the matrix structure resulting from the mix of field and interface variables in this free-boundary problem.

One of the most difficult aspects of the numerical problem was obtaining sufficiently accurate first approximations for convergence of Newton's method in the presence of the yield surfaces. We did this by constructing a fictitious free-boundary problem

for the conditions $P_R \to \infty$ and $Y_g = 0.1$ where the velocity and pressure fields are exactly the results for Stokes flow and the shapes of the yield surfaces are found from the conditions that τ on the surface is a constant and the velocity profiles are specified exactly to the Stokes solution. From this first guess, first-order continuation (Brown, Scriven & Silliman 1980) in the composite parameter $\hat{P}_R \equiv 3C_s/P_R$ was used to move continuously in the parameter space toward a solution for the Bingham plastic as $\hat{P}_R$ became large ($P_R \to 0$). Calculations of the drag coefficient and the shape of the outer yield surface with $Y_g = 0.1$ and $\hat{P}_R$ up to 1×10^6 are shown in figure 4 for mesh B2. Based on the convergence of these results, we used the highest value of $\hat{P}_R$ in all subsequent calculations, where different values of the yield stress were obtained using continuation in Y_g.

The stream function $\psi(r, \theta)$ is computed by finite-element solution of the equation

$$\nabla^2\psi = 2 - 3v_\theta \sin\theta + 2v_r \cos\theta + \sin\theta \left(\frac{\partial v_r}{\partial\theta} - r\frac{\partial v_\theta}{\partial r}\right), \tag{3.10}$$

where the stream function is defined by

$$v_r \equiv \frac{1}{r^2 \sin\theta}\frac{\partial\psi}{\partial\theta}, \quad v_\theta \equiv -\frac{1}{r\sin\theta}\frac{\partial\psi}{\partial r}. \tag{3.11}$$

4. Finite-element results

The range of yield stress, measured by Y_g, between an arbitrarily low value (0.001) and values close to the limiting value $Y_g = Y_{g\ell}$ for a motionless sphere have been computed using the finite-element meshes listed in table 1. The calculations using the coarser meshes B1 and B2 were performed on the Honeywell 6180 computer at MIT. Calculations with mesh B3 were performed on the Cray-1S computer at Los Alamos Scientific Laboratory. The discretizations B1 and B2 give the same results for the range $0.1 \leqslant Y_g \leqslant 0.13$; however, the formation of a plastic boundary layer next to the sphere for higher values of Y_g made the calculations inaccurate with the coarser mesh. Calculations with the mesh B2 were continued to $Y_g = 0.135$. The finest mesh B3 was used to examine the solution behaviour as Y_g approached zero. The accuracy of the finite-element results was assessed by comparing the values of the variational integrals $H \equiv H^*/\pi\eta_0 R_0 V_0^2$ and $K \equiv K^*/\pi\eta_0 R_0 V_0^2$ with each other and with the more approximate calculations of Yoshioka *et al.* (1971). The values of the two integrals computed from the finite-element solutions are indistinguishable when plotted as functions of the Bingham number, shown as figure 5. Values of the integrals computed from the finite-element solutions are given in table 2. The results of Yoshioka *et al.* had a large difference between the upper and lower bounds. The values of the integrals computed from our finite-element results consistently fall on or near the value of H computed from the earlier analysis for $N_B > 1$. The finite-element results for the drag coefficient, velocity fields and yield surfaces and the convective mass-transfer coefficient are presented below.

4.1. *Drag coefficient*

The dependence of the drag coefficient on the yield-stress parameter Y_g is shown in figure 6. The drag coefficient tended to infinity, i.e. the sphere ceased to move at a value of Y_g where the yield forces balanced the effects of gravity. The value for this limit $Y_{g\ell} \approx 0.143$ has been computed using the correlation between C_s and Y_g derived by the plastic boundary-layer analysis presented in §5.

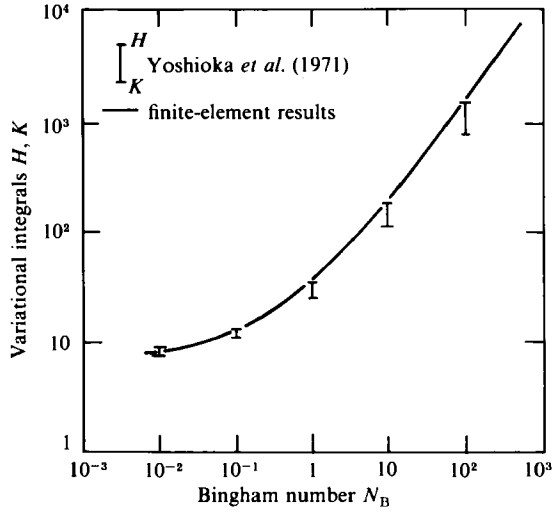

FIGURE 5. Comparison of values of variational integrals H and K computed using the finite-element method (——) and the approximate methods of Yoshioka *et al.* (1971). The values of the integrals H and K computed using the finite-element results are indistinguishable. The error bars for the approximate calculations indicate the difference between H (upper bound) and K (lower bound) respectively.

Y_g	N_B	C_s	H	K	$N_{Sh}N_{Pe}^{-\frac{1}{3}}$	$f_1(0)$	θ_1	$f_2(0)$	$f_2(\frac{1}{2}\pi)$
0†	0	1	6.00	6.00	1.00	0	0	∞	∞
0.001	0.007	1.17	7.37	7.36	1.041	1.000	0	23.19	33.10
0.01	0.108	1.74	12.41	12.41	1.169	1.003	0.010	7.331	10.59
0.036	0.747	3.46	28.97	28.96	1.379	1.016	0.052	3.781	5.520
0.06	2.299	6.39	59.44	59.38	1.570	1.031	0.086	2.806	4.134
0.088	8.047	15.24	156.65	156.65	1.857	1.051	0.149	2.188	3.250
0.1	14.91	24.85	265.25	265.25	2.031	1.052	0.180	2.038	3.013
0.11	27.36	41.45	455.97	456.06	2.223	1.060	0.204	1.900	2.813
0.12	59.59	82.77	937.95	937.83	2.503	1.069	0.232	1.765	2.626
0.13	197.5	253.2	2950.1	2948.3	3.024	1.080	0.264	1.637	2.439
0.133	340.7	426.9	5031.0	5021.8	3.301	1.084	0.276	1.591	2.373
0.135	544.6	672.3	7942.1	7899.3	3.557	1.087	0.287	1.555	2.322

† Exact results from Stokes solution.

TABLE 2. Solution parameters for selected values of Y_g. Parameter values used in calculations were as follows. Mesh B1: $0.04 \leqslant Y_g < 0.100$, $\lambda = 10^5$, $\hat{P}_R = 10^5$. Mesh B2: $0.100 \leqslant Y_g < 0.117$, $\lambda = 10^5$, $\hat{P}_R = 10^6$; $0.117 \leqslant Y_g < 0.130$, $\lambda = 10^6$, $\hat{P}_R = 10^6$; $0.130 \leqslant Y_g \leqslant 0.135$, $\lambda = 4 \times 10^6$, $\hat{P}_R = 10^6$. Mesh B3: $0.001 \leqslant Y_g \leqslant 0.04$, $\lambda = 10^6$, $\hat{P}_R = 10^5$.

The numerically computed values of drag coefficient for low values of Y_g reached nearly a constant slope except for very small values of Y_g where a rapid transition occurred to the value of C_s for a sphere falling in a Newtonian fluid. The finite-element results are compared in figure 7 to the experimental measurements of Ansley & Smith (1967) as a function of the Bingham number N_B. The agreement is good considering the limited reproducibility of the experimental results. The upper and lower bounds computed from the variational integrals by Yoshioka *et al.* (1971) are shown again for reference.

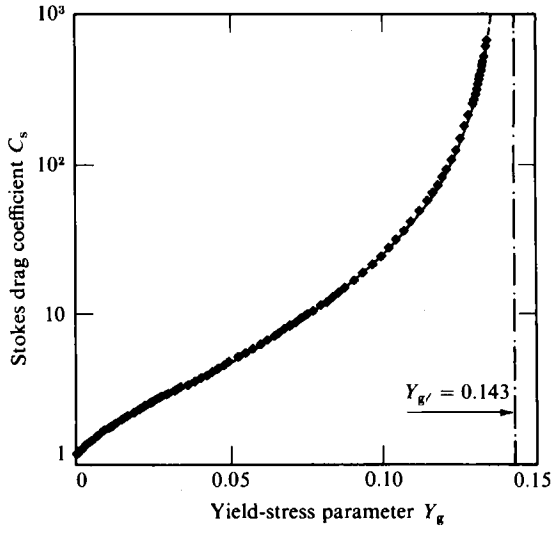

FIGURE 6. Dependence of the Stokes drag coefficient on the yield-stress parameter Y_g.

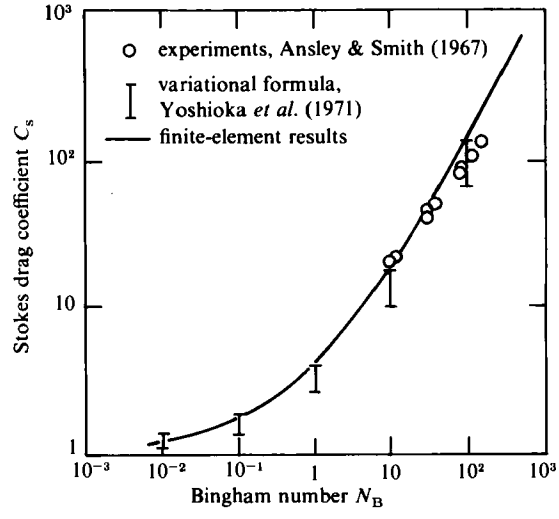

FIGURE 7. Dependence of Stokes drag coefficient on the Bingham number. Finite-element results are represented by the continuous curve and the experimental data of Ansley & Smith (1967) by (○). The upper and lower bounds calculated by Yoshioka *et al.* (1971) are shown as error bars.

4.2. *Velocity fields and yield surfaces*

The streamlines computed for four values of the yield-stress parameter Y_g are shown in figure 8. Streamlines are only shown inside the fluid region for $Y_g \neq 0$, but extend as straight vertical lines in the solid, corresponding to rigid translation of this material when viewed from the sphere. For $Y_g = 0$ the fluid region extends to infinity and the streamlines are never straight. For the lowest value of Y_g (0.036), the streamlines are quantitatively different from the Stokes solution everywhere in the fluid region; this is especially evident from comparing the spacing of the streamlines along the symmetry plane $\theta = \frac{1}{2}\pi$. The outer yield surface for this yield stress is approximately $4R_0$ away from the sphere at this symmetry plane. The angle of departure for the outer yield

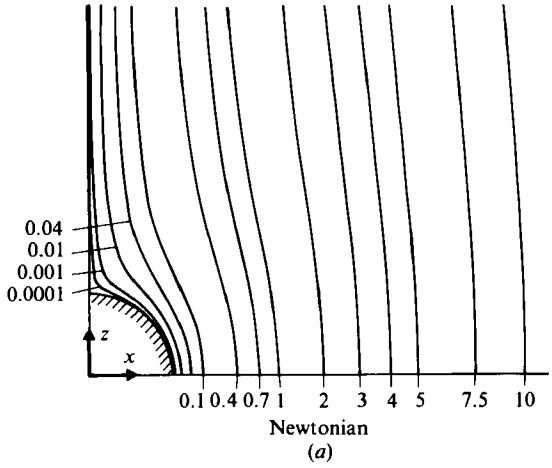

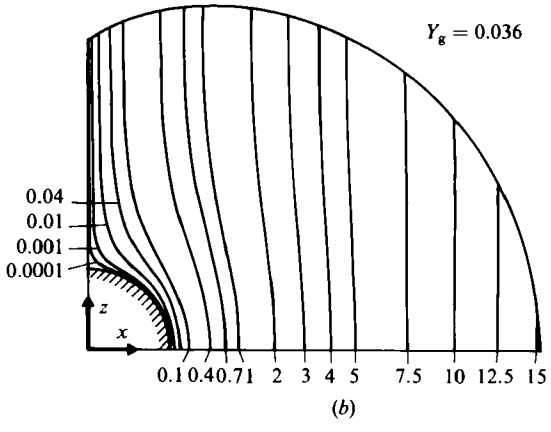

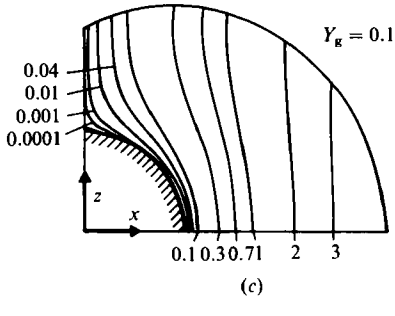

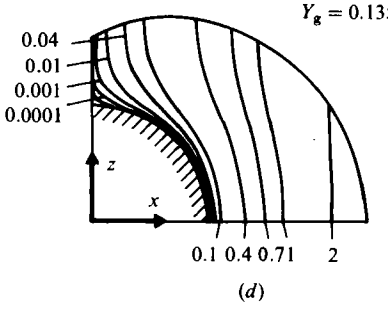

FIGURE 8. Streamlines for flow around a sphere for (*a*) Stokes flow ($Y_g = 0$); (*b*) $Y_g = 0.036$; (*c*) 0.1; (*d*) 0.135. Streamlines are only shown inside the plastic region for cases with non-zero yield stress, and should be continued as vertical lines in the rigid solid.

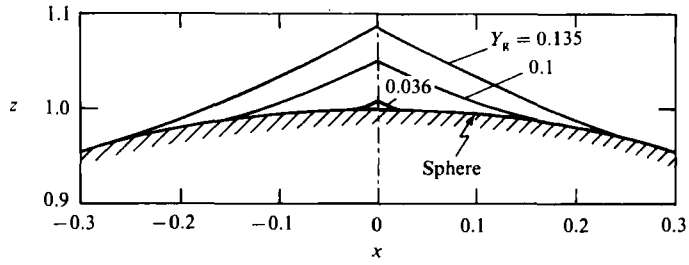

FIGURE 9. Shapes of the polar solid caps for the three non-zero values of Y_g listed in figure 8.

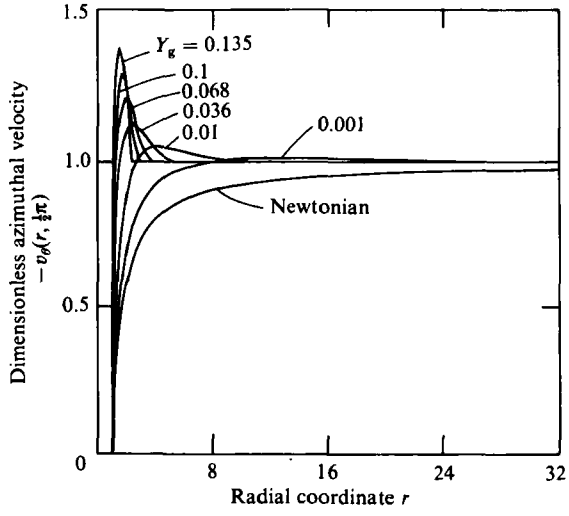

FIGURE 10. Radial profiles of the azimuthal velocity field at $\theta = \frac{1}{2}\pi$ for several values of Y_g and for Stokes flow.

surface at the top and bottom of the sphere is nearly $\frac{1}{4}\pi$, as suggested by the theory for planar slip lines of Slater (1977) for the angle of intersection of a slip line with a plane of symmetry. The solid cap at the top of the sphere is just visible in the plots for the largest two values of Y_g; these caps are shown separately in figure 9.

Increasing the yield-stress parameter Y_g decreased the size of the fluid region, as demonstrated by figures 8(*c*) and (*d*), which are drawn on the same scale as (*a*) and (*b*). The flow pattern near the sphere stays approximately the same with increasing yield stress, except for an increase in the steepness of the velocity gradient next to the solid, suggesting the formation of a boundary layer. Increasing the yield-stress parameter Y_g closer to its limiting value, or equivalently computing for very large values of N_B, is not expected to change the shape of the outer yield surface appreciably. Instead, the yield surfaces reach limiting shapes, similar to the results for $Y_g = 0.135$ ($N_B = 700$) with the outer surface detached from the sphere. Surprisingly, Ansley's picture of the outer surface as a toroid is close to this finite-element calculation.

The formation of the boundary layer is better seen in the radial profiles of the angular velocity v_θ at $\theta = \frac{1}{2}\pi$ shown in figure 10 for several values of Y_g. The qualitative difference between the profiles for non-zero yield stress and the Newtonian result is striking. The presence of the outer yield surface causes the azimuthal velocity

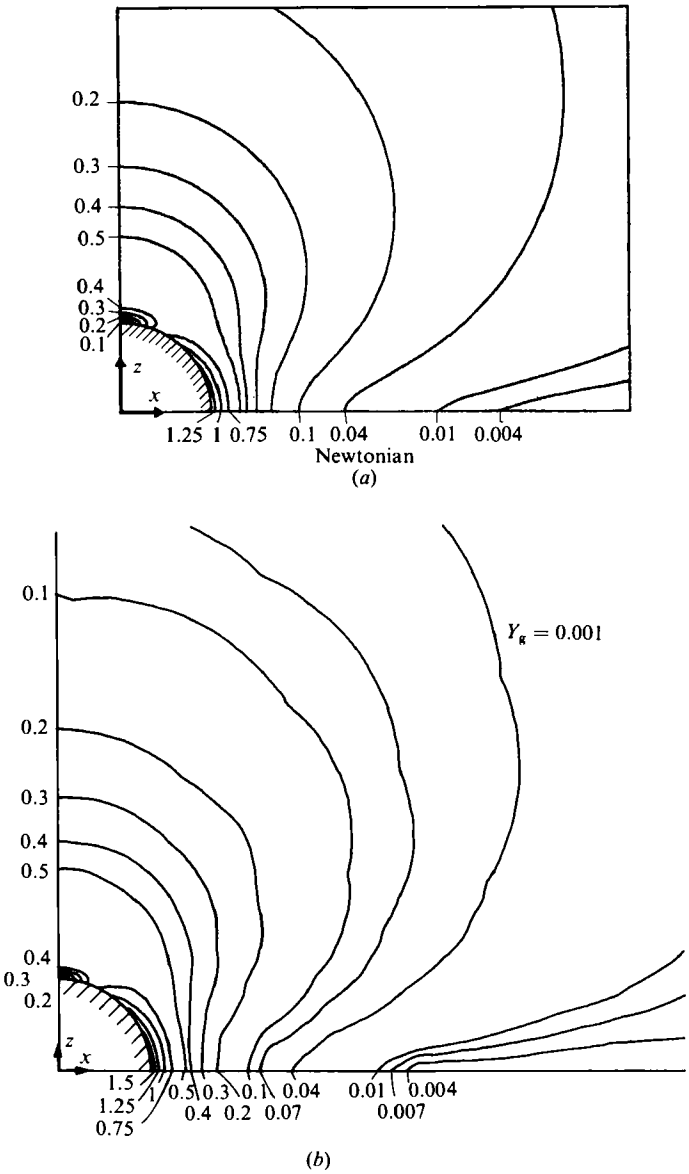

FIGURE 11. Contours of the second invariant of the rate-of-strain tensor $\dot{\gamma}$ (*a*) for Stokes flow; and for the Bingham results with (*b*) $Y_g = 0.001$; (*c*) 0.01; (*d*) 0.036; (*e*) 0.1. The scale of the lengths in the last case has been magnified by a factor of two to show the detail.

to go through a minimum between the sphere and this surface in order to conserve mass. This minimum is not present for $Y_g = 0$, where the velocity goes monotonically from zero at the sphere to -1 as $r \to \infty$. The velocity minimum increases and the gradient sharpens as the yield stress approaches the critical value for the just static sphere. The velocity minimum decreased and shifted to larger values of r as the yield stress was decreased. The singularity in the velocity field associated with the approach to the Stokes limit is evident from figure 10. For $Y_g = 0.001$ the slope $\partial v_\theta / \partial r$ is similar to the Newtonian curve, but the magnitude of the velocity is shifted because of the effect of the plastic portion of the viscosity on the flow away from the sphere.

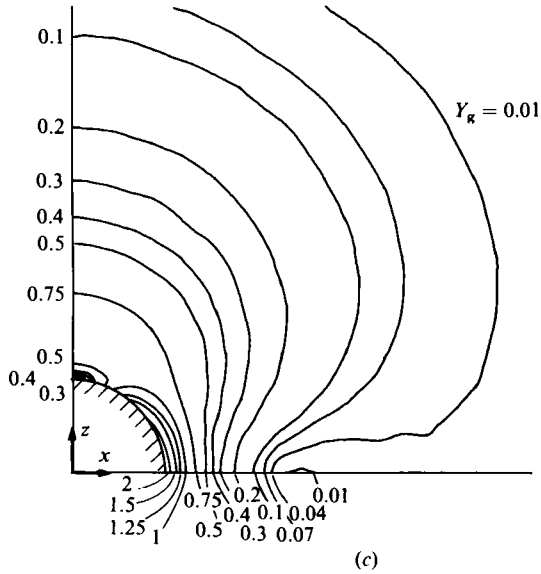

(*c*)

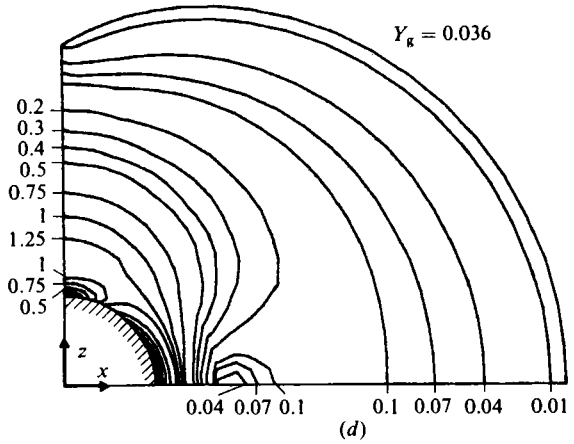

(*d*)

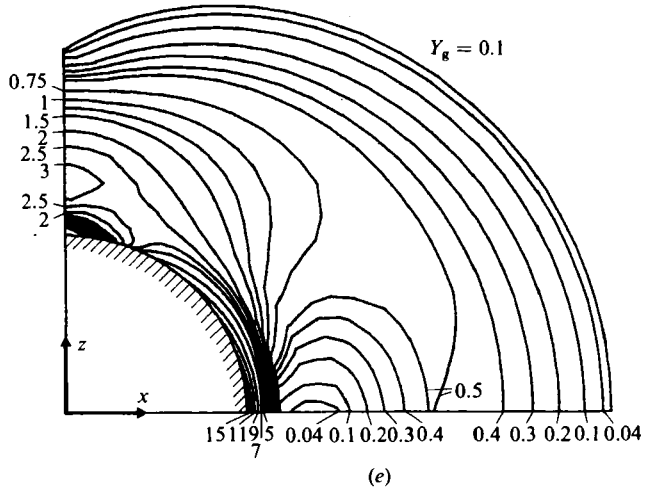

(*e*)

FIGURE 11 (*c*)–(*e*). For caption see opposite page.

The flow field differs from the Newtonian solution for most of the flow domain, even when the drag coefficient approaches the Stokes limit. These differences are explained more precisely by the matched asymptotic analysis presented in §5.2.

Contours of the second invariant of the rate-of-strain tensor $\dot{\gamma}$ are shown in figure 11 for the Newtonian- and Bingham-fluid models. All the profiles are smooth, indicating the quality of the numerical approximations to the velocity field and its gradients. The minimum in the angular velocity for the Bingham-fluid profile causes a qualitative difference in the rate-of-strain contours for the two models. For a Bingham fluid a small torus centred on the symmetry plane exists where $\dot{\gamma}$ is small relative to the values slightly closer to the sphere. For a fluid particle the motion in this torus is close to the sum of a rigid translation in the direction of flow and solid-body rotation, driven by the high shear rates experienced closer to the surface of the sphere. A perfectly rigid rotation is impossible in the axisymmetric configuration, except exactly at $\theta = \frac{1}{2}\pi$. The shifting of the velocity minimum away from the sphere with decreasing Y_g is obvious by comparing figures 11 (*d*) and (*e*).

The approach of the flow field for the Bingham fluid to the Stokes result (figure 11 *a*) is shown by figures 11 (*b*) and (*c*), for Y_g values of 0.001 and 0.0103 respectively. The result for the lowest value of the yield stress is quite similar to the Newtonian result over the portion of the flow domain shown ($0 \leqslant r \leqslant 6$). The influence of the plastic portion of the viscosity is limited to distances farther from the sphere. At $Y_g = 0.0103$ the flow field at distances less than two radii from the sphere was altered by the non-Newtonian viscosity and the torus of almost-rigid-body rotation had just appeared.

4.3. *Mass transfer at high Péclet numbers*

The changes in the velocity field adjacent to the sphere have pronounced effects on the predictions of mass and heat transfer from the sphere to the surrounding fluid. To demonstrate this we compute the mass-transfer coefficient for transfer of a dilute species from the surface of the sphere to the surrounding fluid at infinite dilution. The calculation is performed in the limit of high Péclet number $N_{Pe} \equiv V_0 R_0/D$, where D is the mass diffusivity, so that the gradient of concentration is confined to a thin concentration boundary layer adjacent to the sphere. If the shielding of the poles of the sphere by the small solid caps is accounted for, the expression for the Sherwood number reported by Baird & Hamielec (1962) can be used directly as

$$N_{Sh} \equiv 0.641 N_{Pe}^{\frac{1}{3}} \left[\int_{\theta_1}^{\pi-\theta_1} \left[\left| \frac{\partial v_\theta}{\partial r}(1,\theta) \right| \sin^3\theta \right]^{\frac{1}{2}} \mathrm{d}\theta \right]^{\frac{2}{3}}, \tag{4.1}$$

where $N_{Sh} \equiv 2R_0 k_L/D$ in which k_L is the mass-transfer coefficient. Values of $N_{Sh} N_{Pe}^{-\frac{1}{3}}$ computed using the velocity gradients from the finite-element calculations are displayed as figure 12. The Newtonian value of the coefficient 0.991 reported by Baird & Hamielec (1962) is also shown. At the critical yield stress $Y_g \equiv Y_{g\ell} \approx 0.143$, the Péclet number tends to zero faster than the integral and the Sherwood number N_{Sh} approaches zero, as expected.

5. Asymptotic analysis of high and low N_B

5.1. *Plastic boundary-layer theory*

As the yield stress approaches the critical value (either $N_B \to \infty$ or $Y_g \to Y_{g\ell}$) viscous forces, characterized by the viscosity η_0, are important only in a narrow envelope surrounding the sphere where $\dot{\gamma}$ is large. Outside this layer the yield-stress contribution

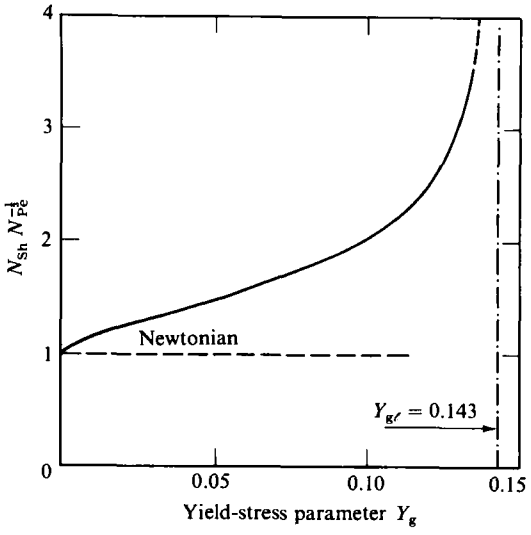

FIGURE 12. Dependence of the product $N_{Sh}\,N_{Pe}^{\frac{1}{3}}$ on the yield-stress parameter Y_g.

to the viscosity dominates the flow, as the stress decreases toward the yield value. Oldroyd (1947*b*) developed a set of plastic boundary-layer equations valid in this limit for planar flows. In this subsection we present a similar analysis for the axisymmetric flow around a sphere. Away from the stagnation points at the poles of the sphere, we rescale the radial variable to account for the thin layer of moving fluid as

$$r = 1 + \zeta\epsilon, \tag{5.1}$$

where $\epsilon \ll 1$ is the thickness of the layer where viscous and yield forces are both important and ζ is the new radial coordinate. In this region the dimensionless azimuthal velocity is $O(1)$ and the radial velocity is $O(\epsilon)$. The appropriate scaling on the Stokes stream function given by (3.11) is

$$\psi(r, \theta) = \epsilon Q(\zeta, \theta), \tag{5.2}$$

where $Q(\zeta, \theta)$ is $O(1)$. The invariant $\dot{\gamma}$ is large in the boundary layer, scaling as

$$\dot{\gamma}(r, \theta) = \epsilon^{-1} G(\zeta, \theta), \tag{5.3}$$

where $G(\zeta, \theta) = O(1)$ and is defined by

$$G(\zeta, \theta) = \frac{1}{\sqrt{2}\sin\theta}\{Q_{\zeta\zeta} - \epsilon(2Q_\zeta + \zeta Q_{\zeta\zeta})\} + O(\epsilon^2), \tag{5.4}$$

with the subscript ζ denoting partial differentiation, i.e. $Q_\zeta \equiv \partial Q/\partial\zeta$.

Substituting (5.2)–(5.4) into the momentum balances (2.1) and constitutive equation (2.3) for the plastic region and making use of the scaling relationship (5.2) gives the following reduced equations:

$$p_\theta = -\frac{1}{\epsilon^2 \sin\theta} Q_{\zeta\zeta\zeta} - N_B\left[\sqrt{2}\,\frac{\partial}{\partial\zeta}\left(\zeta + \frac{Q_\zeta}{2Q_{\zeta\zeta}}\right) + O(\epsilon)\right] + O(\epsilon^{-1}), \tag{5.5}$$

$$p_\zeta = \frac{1}{\sin\theta} Q_{\zeta\zeta\theta} + N_B\left[\frac{\epsilon}{2\sin\theta}\,\frac{\partial}{\partial\zeta}\left(\frac{Q_{\zeta\theta}}{G}\right) + O(\epsilon^2)\right] + O(\epsilon), \tag{5.6}$$

in which the subscript θ denotes $\partial/\partial\theta$. Equations (5.5) and (5.6) are consistent if

$$N_B \epsilon^2 = 1, \tag{5.7}$$

so that the scaling on the pressure is $p(\zeta,\theta)\epsilon^2 = \Pi(\zeta,\theta)$, with $\Pi(\zeta,\theta) = O(1)$. The radial component of the momentum-balance equation (5.6) reduces to the classical boundary-layer result $\partial\Pi/\partial\zeta = O(\epsilon)$, so that at the lowest order of approximation the pressure field in the thin layer of moving fluid is constant with radius. Differentiation of (5.5) with respect to ζ yields a fourth-order equation in terms of the stream function $Q(\zeta,\theta)$, to be solved with boundary conditions that match this flow to motion valid beyond $\zeta = 1$. The structure of the flow outside the plastic boundary layer is connected with the shape of the outer yield surface, and is only known from the solution of the entire free-boundary problem.

Even so, the scalings resulting from the boundary-layer analysis are extremely useful for interpreting the results of the finite-element calculations. It is simple to show that all the components of the extra stress tensor $\boldsymbol{\tau}$ are $O(1)$ in the boundary layer, so that the force exerted on the sphere is dominated by the pressure, which is $O(\epsilon^{-2})$. Then the drag force on the sphere is

$$C_s \equiv \tfrac{1}{3}F \approx \frac{1}{3}\int_0^\pi \Pi(0,\theta)\,\boldsymbol{\delta}_z\cdot\boldsymbol{n}\,\mathrm{d}\theta = \frac{1}{\epsilon^2}\,(a + b\epsilon + O(\epsilon^2)), \tag{5.8}$$

where a and b are constants. Eliminating ϵ from (5.8) using the scaling between the boundary-layer thickness and N_B given in (5.7) and the relationship between N_B and Y_g yields the form for correlating the drag force as

$$C_s \approx \frac{\alpha Y_g}{(\beta - Y_g)^2}, \tag{5.9}$$

where α and β are constants. The critical value of Y_g is predicted by (5.9) as the limit $Y_g \to \beta$.

Similarly, the scaling for the Sherwood number in the boundary-layer regime is derived as

$$N_{Sh}\, N_{Pe}^{-\frac{1}{3}} \sim \epsilon^{-\frac{1}{3}} \sim N_B^{\frac{1}{6}}. \tag{5.10}$$

For a given Bingham number and sphere radius, the definitions of N_B and N_{Pe} give $N_{Pe} \sim N_B^{-1}$. This allows elimination of N_{Pe} from (5.10) to give

$$N_{Sh} \sim N_B^{-\frac{1}{6}}. \tag{5.11}$$

The validity of the scalings (5.7)–(5.11) predicted by the plastic boundary-layer analysis is demonstrated in figure 13. The boundary-layer thickness at $\theta = \frac{1}{2}\pi$, defined as the radial distance for the velocity to change from 0 to -1, is shown as a function of Bingham number in figure 13(*a*). The slope of the best-fit line for the entire range of N_B is -0.57, in good agreement with the boundary-layer result, (5.2), of -0.5. The product $N_{Sh}\, N_{Pe}^{-\frac{1}{3}}$ is plotted as a function of the Bingham number in figure 13(*b*). The slope of the finite-element calculations is 0.16, extremely close to the prediction from the boundary-layer analysis of $\frac{1}{6}$.

The form for the drag coefficient (5.9) can be fitted to the finite-element results for $N_B > 100$ with $\alpha = 1.031$ and $\beta = 0.14334$, and has less than 1 % relative error in the parameter range.

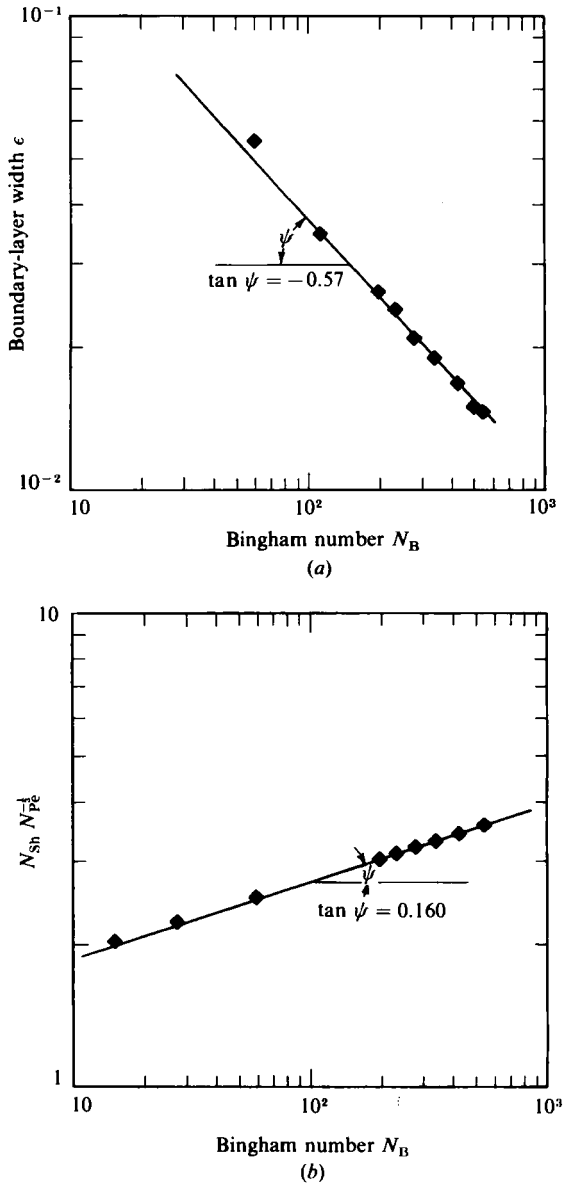

FIGURE 13. Comparison of finite-element results with scalings predicted by plastic boundary-layer theory ($N_B \to \infty$) for (*a*) the width of the boundary layer and (*b*) the product $N_{Sh}\, N_{Pe}^{-\frac{1}{3}}$. The finite-element calculations are represented by the symbols (◆); the curves are least-square regressions of these results.

5.2. *Asymptotic expansion for low* N_B

The rapid decrease of the drag coefficient to the Newtonian value as $N_B \to 0$ signals a change in the characteristic scaling from the one predicted by (5.9) and the plastic boundary-layer theory. The scaling valid for $N_B \ll 1$ is found by a matched asymptotic analysis similar to the one used for low-Reynolds-number flow around a sphere (Proudman & Pearson 1957; Van Dyke 1964). We are indebted to J. F. Brady for his assitance in this analysis.

The Stokes velocity field for a Newtonian fluid,

$$v_r = -\frac{\cos\theta}{2r^2}\left[\frac{1}{r} - 3r\right], \quad v_\theta = -\frac{\sin\theta}{4r^2}\left[3 + \frac{1}{r^2}\right], \tag{5.12}$$

is not uniformly valid for large r away from the sphere for any non-zero value of N_B because the plastic correction to the viscosity, $N_B/2\dot{\gamma}$, in (2.3) becomes larger than the Newtonian contribution. By analogy with the low-Reynolds-number problem, there must be an inner region near the sphere where (5.12) holds, and an outer region adjoining the yield surface where the plastic portion of the viscosity becomes important. In the following analysis we derive the proper scalings for the velocity field and drag coefficient valid in this limit. For simplicity, we neglect the presence of the solid caps at the poles of the sphere. These shrink uniformly with decreasing N_B and should not play a dominant role in the scalings for the flow.

Substituting the Stokes velocity field (5.12) into the viscosity expression (2.3) for the Bingham fluid and forcing both the Newtonian and plastic terms to be of equal importance suggest rescaling the radial coordinate as

$$r^* = rN_B^{\frac{1}{2}} \tag{5.13}$$

away from the sphere. Then the equation set in this outer region becomes

$$\nabla\cdot\left[\left(1 + \frac{1}{2\dot{\gamma}^*}\right)\dot{\gamma}^*\right] = \mathbf{0}, \tag{5.14}$$

$$\dot{\gamma}^* = v_\theta^* = v_r^* = 0 \quad \text{on } \partial\hat{D}_{2,b}, \tag{5.15}$$

where (v_r^*, v_θ^*) are velocity components scaled with $VN_B^{\frac{1}{2}}$ and $\dot{\gamma}^*$ is the second invariant of the rate of strain computed with the rescaled variables. The solution of the free-boundary problem (5.12)–(5.15) must be matched to the Stokes result written in the outer variable for $r^* \ll 1$. Higher-order approximations are computed as a Taylor series in $\epsilon = N_B^{\frac{1}{2}}$ in a fashion analogous to that presented by Van Dyke (1964). Unfortunately, the outer problem defined here is a nonlinear free-boundary problem of similar difficulty to the entire problem solved in §4. Hence we will only use the asymptotic analysis to compute the correct scalings as $N_B \to 0$, and will not pursue the calculation of the coefficients.

The dominant dependence of the drag coefficient on the Bingham number is recovered by considering the $O(N_B^{\frac{1}{2}})$ correction to the flow near the sphere. Because the plastic term in the viscosity is still small to this order of approximation, the correction, which is no more singular than the Stokes velocity field, is easily computed as

$$v_\theta^{(1)} = \epsilon\frac{C_2}{4}\sin\theta\left(4 - \frac{3}{r} - \frac{1}{r^2}\right), \tag{5.16}$$

$$v_r^{(1)} = \epsilon\frac{C_2}{2}\cos\theta\left(2 - \frac{3}{r} + \frac{1}{r^2}\right), \tag{5.17}$$

where the constant C_2 must be determined by matching this solution to the outer solution for $r^* \ll 1$. At large values of r (5.16) reduces to a uniform velocity of magnitude ϵC_2, which describes the overshoot observed in the velocity profile (see figure 10) due to the finite size of the flow domain for non-zero N_B.

The leading-order correction to the drag coefficient is computed from the inner solution as

$$C_s = 1 + N_B^{\frac{1}{2}} C_2. \tag{5.18}$$

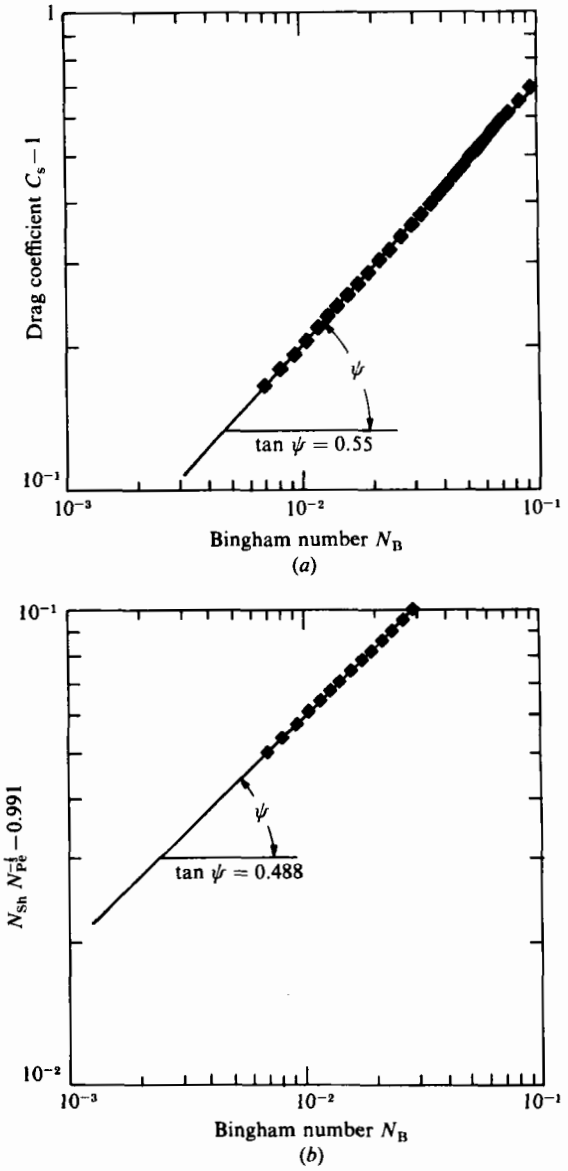

FIGURE 14. Comparison of finite-element results with scalings predicted by the asymptotic theory ($N_B \to 0$) for (*a*) the drag coefficient and (*b*) the product $N_{Sh} N_{Pe}^{-\frac{1}{3}}$. The finite-element calculations are represented by the symbols (◆); the curves are least-square regressions of these results.

The scaling of the Sherwood number for large Péclet number is derived from (4.1) as

$$N_{Sh} N_{Pe}^{-\frac{1}{3}} \sim 0.991 + C_4 N_B^{\frac{1}{2}}, \tag{5.19}$$

where the leading coefficient has been computed from the analysis of Baird & Hamilelec (1962) for a sphere in Stokes flow and C_4 is an undetermined constant.

The validity of the scalings in (5.18) and (5.19) for $N_B \ll 1$ is demonstrated in figure 14. The best-fit line through the finite-element results for $0.007 \leqslant N_B \leqslant 0.012$ is

$$\ln (C_s - 1) = 0.91 + 0.55 \ln N_B, \tag{5.20}$$

in good agreement with (5.18). The product $N_{Sh} N_{Pe}^{-\frac{1}{3}}$ is plotted as a function of N_B in figure 14(*b*). The slope of the finite-element calculations in the range $0.007 \leqslant N_B \leqslant 0.012$ is 0.48, close to the result of $\frac{1}{2}$ predicted by the asymptotic analysis.

5.3. *Composite expansions for drag and mass-transfer coefficients*

The scalings predicted by the analyses in §§5.1 and 5.2 for high and low values of N_B have been used to develop a composite scaling for correlating C_s and N_{Sh} over the entire range of yield stress. The scaling (5.8), for the drag coefficient at large Y_g, is rewritten in terms of N_B as

$$C_s = a_1 N_B + a_2 N_B^{\frac{1}{2}} + O(1), \tag{5.21}$$

where a_1 and a_2 are constants. A rigorous joining of the series (5.18) and (5.21) is possible only if one of the series is convergent for the whole range of N_B (Van Dyke 1964). Since the exact structure of each series cannot be guaranteed, we proceed only by examining a composite expansion formed by adding the results for high and low N_B as

$$C_s = 1 + a_3 N_B^{\frac{1}{2}} + a_4 N_B + \text{higher-order terms}, \tag{5.22}$$

which is uniform in the sense that it contains the leading-order information from each asymptotic expansion.

The constants are determined by fitting exactly the finite-element results at the lowest ($N_B = 0.007$, $C_s = 1.167$) and highest ($N_B = 544.590$, $C_s = 672.33$) values of yield stress available. The resulting parameters $a_3 = 1.874$ and $a_4 = 1.152$ give a correlation for the drag coefficient that is accurate to within 2.5 % of the finite-element results for the entire range of N_B. The greatest error occurs at $N_B \approx 14$, where neither of the asymptotic results can be expected to hold.

The asymptotic results (5.10) and (5.19) for the Sherwood number for low and high values of N_B suggest that a composite correlation of the form

$$N_{Sh} N_{Pe}^{-\frac{1}{3}} = C_5 (1 + C_6 N_B^{\frac{1}{2}} + C_7 N_B)^{\frac{1}{6}}, \tag{5.23}$$

be fitted to the finite-element results over the entire range of N_B by adjusting the constants C_5, C_6, C_7. These constants can be determined solely by forcing (5.23) to reduce to (5.10) and (5.19) in the appropriate limits; the resulting constants $(C_5, C_6, C_7) = (0.9915, 3.631, 3.663)$ gave a maximum relative error of 10 % between the correlation (5.23) and the finite-element results for the entire range of N_B. Simply fitting the three constants in (5.23) to the calculations for $N_B = 0$, 0.1 and 544.5 gave $(C_5, C_6, C_7) = (0.9915, 3.79076, 3.75241)$ and produced a maximum relative error of only 0.5 %. Again the maximum deviation occurred near $N_B = 14$.

6. Conclusions

Numerical solution of viscoplastic flows as properly posed free-boundary problems is a powerful approach to analysis of complex problems, because it yields the precise shape and number of the yield surfaces, and gives efficient allocation of computational power, by restricting the calculation to only the fluid or plastic region of the material. The finite-element/penalty formulation used here also allows systematic mesh refinement near the yield surfaces for improved accuracy and efficiency. The quality of the solutions presented is high, as brought out by the calculation of the variational integrals. These results should replace the very approximate calculations that have appeared before for flow around a sphere.

The computed values of the drag coefficient presented in table 1, in figure 6 and in the correlations in §5 can be used to determine the material properties τ_y and η_0 from measured values of the terminal velocities for falling spheres. This measurement does not rely on measuring the yield stress directly at the point for cessation of motion, as is the case for measurements based on simpler rectilinear-flow solutions (see Bird *et al.* 1983). Falling-sphere viscometry may be more accurate, especially for materials with low yield stress.

Calculations for the range of yield-stress parameter have pointed out two interesting features of the flows occurring at the opposite ends of the accessible values of yield stress. First, at high values of the Bingham number, the motion near the sphere and the drag force on it are described well by a plastic boundary-layer theory that accounts for the contributions of both the viscous and yield forces to the force balance in a thin layer near the sphere. This approach is extremely useful for determining the scalings for variables near the critical yield stress, but cannot simply yield closed-form results, because of the unknown matching conditions between this layer and the fluid adjacent to it that has its motion dominated by the yield-stress contribution to the viscosity. The finite-element calculations indicate that the scalings for the drag and mass-transfer coefficients predicted by the boundary-layer theory are valid for all Bingham numbers greater than 0.6.

Calculations for decreasing yield stress indicated a change in scaling below $N_B \approx 0.6$. For lower values of N_B the flow field reduced to a Newtonian region surrounding the sphere and a region where the fluid was viscoplastic far from it. A matched asymptotic expansion gave the correction to the drag coefficient to be $O(N_B^{\frac{1}{2}})$ for $N_B \ll 1$. Up to this order of approximation the only influence of the plastic viscosity and the outer yield surface was to increase the drag of the sphere through a uniform increase in the velocity field away from the sphere. Small changes in N_B led to larger changes in C_s for small yield stresses. The regular perturbation analysis in N_B about the Newtonian flow used by Bhavaraju *et al.* (1978) was inappropriate because it neglected the role of the viscoplastic region away from the sphere in setting the magnitude of the flow adjacent to it.

Small solid caps at the poles of the sphere formed because of the stagnation flow in this region. The caps grew with increasing yield stress. The agreement between the correlations for these coefficients based on the analyses neglecting these solid regions and the finite-element results suggested that these extra yield surfaces played only minor roles in setting the scalings for the flow and transport fields.

This research was supported by the Fluid Mechanics Program of the National Scicnce Foundation, by the Office of Naval Research and by a grant from the Department of Energy for use of computer facilities at Los Alamos Scientific Laboratory.

REFERENCES

ADACHI, K. & YOSHIOKA, N. 1973 On the creeping flow of a viscoplastic fluid past a circular cylinder. *Chem. Engng Sci.* **28**, 215–226.

ANDRES, V. T. 1960 Equilibrium and motion of a sphere in a viscoplastic fluid. *Dokl. Akad. Nauk SSSR* **133**, 777–780.

ANSLEY, R. W. & SMITH, T. N. 1967 Motion of spherical particles in a Bingham plastic. *AIChE J.* **13**, 1193–1196.

BAIRD, M. H. I. & HAMILELEC, A. E. 1962 Forced convection transfer around spheres at intermediate Reynolds numbers. *Can. J. Chem. Engng* **40**, 119–121.

BERCOVIER, M. & ENGELMAN, M. 1979 A finite element method for the numerical solution of viscous incompressible flows. *J. Comp. Phys.* **30**, 181–201.

BERCOVIER, M. & ENGLEMAN, M. 1980 A finite element method for the incompressible non-Newtonian flows. *J. Comp. Phys.* **36**, 313–326.

BHAVARAJU, S. M., MASHELKAR, R. A. & BLANCH, H. W. 1978 Bubble motion and mass transfer in non-Newtonian fluids. *AIChE J.* **24**, 1063–1069.

BINGHAM, E. C. 1922 *Fluidity and Plasticity*, pp. 215–218. McGraw-Hill.

BIRD, R. B., ARMSTRONG, R. C. & HASSAGER, O. 1977 *Dynamics of Polymeric Liquids*, vol. 1. Wiley.

BIRD, R. B., DAI, G. C. & YARUSSO, B. J. 1983 The rheology of flow of viscoplastic materials. *Rev. Chem. Engng* **1**, 1–70.

BROWN, R. A., SCRIVEN, L. E. & SILLIMAN, W. J. 1980 Computer-aided analysis of nonlinear problems in transport phenomena. In *New Methods in Nonlinear Dynamics* (ed. P. Holmes), pp. 289–307. SIAM.

DY PLESSIS, M. P. & ANSLEY, R. W. 1967 Setting the parameters in solids pipelining. *J. Pipeline Div. ASCE* **93**, 1–17.

DUVAUT, G. & LIONS, J. L. 1976 *Inequalities in Mechanics and Physics*. Springer.

ETTOUNEY, H. M. & BROWN, R. A. 1983 Finite element methods for steady solidification problems. *J. Comp. Phys.* **49**, 118–150.

GLOWINSKI, R., LIONS, J. L. & TREMOLIERS, R. 1981 *Numerical Analysis of Variational Inequalities*. North-Holland.

HILL, R. 1950 *The Mathematical Theory of Plasticity*. Oxford University Press.

HOOD, P. 1976 Frontal solution program for unsymmetric matrices. *Intl J. Num. Meth. Engng* **10**, 379–399.

HUGHES, T. J. R., LIU, W. K. & BROOKS, A. 1979 Finite element analysis of incompressible viscous flows by the penalty function formulation. *J. Comp. Phys.* **30**, 1–40.

ITO, S. & KAJIACHI, T. 1969 Drag force on a sphere moving in a plastic solid. *J. Chem. Engng Japan* **2**, 19–24.

LIPSCOMB, G. G. & DENN, M. M. 1984 Flow of Bingham fluids in complex geometries. *J. Non-Newt. Fluid Mech.* **14**, 337–346.

OLDROYD, J. G. 1947*a* A rational formulation of the equations of plastic flow for a Bingham solid. *Proc. Camb. Phil. Soc.* **43**, 100–105.

OLDROYD, J. G. 1947*b* Two-dimensional plastic flow of a Bingham solid. A plastic boundary-layer theory for slow motion. *Proc. Camb. Phil. Soc.* **43**, 383–395.

PRAGER, W. 1954 On slow viscoplastic flow. In *Studies in Mathematics and Mechanics: R. von Mises Presentation Volume*, pp. 208–216. Academic.

PROUDMAN, I. & PEARSON, J. R. A. 1957 Expansions at small Reynolds number for the flow past a sphere and a circular cylinder. *J. Fluid Mech.* **2**, 237–262.

SLATER, R. A. 1977 *Engineering Plasticity*, pp. 182–236. Wiley.

SYMONDS, P. S. 1949 On the general equations of problems of axial symmetry in the theory of plasticity. *Q. Appl. Maths* **6**, 448–452.

VALENTIC, L. & WHITMORE, R. L. 1965 The terminal velocity of spheres in Bingham plastics. *Brit. J. Appl. Phys.* **16**, 1197–1203.

VAN DYKE, M. 1964 *Perturbation Methods in Fluid Mechanics*. Academic.

VOLAROVICH, M. P. & GUTKIN, A. M. 1953 Theory of flow in a viscoplastic medium. *Colloid J.* **15**, 153–159.

YOSHIOKA, N. & ADACHI, K. 1971 On variational principles for a non-Newtonian fluid. *J. Chem. Engng Japan* **4**, 217–220.

YOSHIOKA, N., ADACHI, K. & ISHIMURA, H. 1971 On creeping flow of a viscoplastic fluid past a sphere. *Kagaku Kogaku* **10**, 1144–1152.